Materials Science in Semiconductor Processing 155 (2023) 107231

Contents lists available at ScienceDirect

Materials Science in Semiconductor Processing

journal homepage: www.elsevier.com/locate/mssp

A novel passivating contact approach for enhanced performance of crystalline silicon solar cells

Muhammad Quddamah Khokhar [a], Shahzada Qamar Hussain [b], Youngkuk Kim [a,c], Suresh Kumar Dhungel [c,**], Junsin Yi [a,c,*]

[a] Department of Electrical and Computer Engineering, Sungkyunkwan University, Suwon, Gyeonggi-Do, 16419, Republic of Korea
[b] Department of Physics, COMSATS University Islamabad, Lahore Campus, Lahore, 54000, Pakistan
[c] College of Information and Communication Engineering, Sungkyunkwan University, Gyeonggi-Do, 16419, Republic of Korea

ARTICLE INFO

Keywords:
TOPCon solar cell
Passivated contact
Nanocrystalline silicon oxide
Tunnel oxide

ABSTRACT

Passivated contacts based on ultrathin silicon oxide (SiO_x) layers and phosphorus-doped nanocrystalline silicon oxide (nc-SiO_x(n)) layers have been examined for their application in tunnel oxide-passivated contact (TOPCon) solar cells. Passivated contact nc-SiO_x(n)/SiO_x, is accomplished by implementing a thermally grown SiO_x tunnel layer and a plasma-enhanced chemical vapor deposited (PECVD)-grown nc-SiO_x(n) layer, which are subsequently transformed into a more crystalline phase by annealing at a higher temperature. In this research, a 3.2 × 3.2 cm solar cell was fabricated, where the base material was n-type crystalline silicon (c-Si(n)), and an aluminum oxide (Al_2O_3) acts as a passivation layer which helps to enhanced the passivation properties and indium tin oxide (ITO) layer was used on the front side, which could serve as an anti-reflection coating (ARC), respectively. The influence of the temperature, doping level, and thickness of nc-SiO_x(n) on the surface passivation of the contacts was investigated. Superior recombination current density (J_o) values of up to 2.9 fA/cm^2 were assessed for the nc-SiO_x(n)/SiO_x contacts. TOPCon solar cells with top boron-doped emitter, Al_2O_3, and ITO/rear stack of nc-SiO_x(n)/SiO_x passivation contacts were formed and resulted in V_{oc} = 650 mV and FF = 78%. Furthermore, we focused on ameliorating the achievements of solar cells using a transparent passivating contact-based nc-SiO_x(n), as well as the passivation process and operating principle.

1. Introduction

In recent years, carrier-selective contacts (CSC) have significantly enhanced the performance of c-Si solar cells. Heterojunction solar cells is considered a popular technology, in which hydrogenated amorphous silicon (a-Si:H) layers allow for small surface recombination velocities, along with remarkable V_{oc} values of 750 mV [1]. A fine SiO_x layer stacked with a doped silicon film (such as poly-Si, semi-insulator polycrystalline silicon (SIPOS) [2], TOPCon [3], and Hybrid [4]) is another intriguing notion, known as passivated contact. The efficiency of an n-type silicon solar cell using front boron diffused with tunnel oxide passivated back contact was previously determined to be 25.1% [5], matching the biggest achievement in favor of solar cells with top/rear contacts as set by Daisuke et al. [6]. Because all silicon-based CSC lead to large parasitic absorption losses across the blue wavelength region, it is advisable to individually position all CSC polarities on the back side. As a consequence of incorporating particular a-Si/c-Si heterojunctions within an interdigitated back contact (IBC) solar cell structure, a record holder efficiency in favor of Si solar cells of 25.6% was achieved [7]. However, the production of such solar cells requires intricate patterning techniques. However, employing poly-Si layers and masked ion implantation can make the procedure simpler to produce IBC solar cells. In IBC silicon solar cells, an ion implantation was used to generate passivated contacts [8–12]. These methods involve very complex steps for cell fabrication and use semicrystalline silicon films or polycrystalline silicon films with a thickness of more than 100 nm. A higher film thickness causes parasitic absorption losses in the silicon solar cell, and the complex and extra fabrication steps increase the cost.

This research is aimed at obtaining an innovative solar cell design that uses nc-SiO_x(n)/SiO_x contacts in the rear, along with boron-doped emitter/Al_2O_3/ITO contacts on the top surface. ITOs, used as the top layer of crystalline silicon solar cells, can be additionally used as

* Corresponding author. 2066, Seobu-ro, Jangan-gu, Suwon, 16419, Gyeonggi-Do, Republic of Korea.
** Corresponding author. 2066, Seobu-ro, Jangan-gu, Suwon, 16419, Gyeonggi-Do, Republic of Korea.
E-mail addresses: suresh@skku.edu (S.K. Dhungel), junsin@skku.edu (J. Yi).

https://doi.org/10.1016/j.mssp.2022.107231
Received 21 August 2022; Received in revised form 4 November 2022; Accepted 15 November 2022
Available online 30 November 2022

emitters. Front contacts may readily draw a desirable amount of current from the cell because the ITOs have strong anti-reflective and conductivity properties, reducing the need for anti-reflection coating (ARCs) [13]. The mismatch losses of the solar cell were reduced by the automatically produced SiO_x layer, which served as an interfacial layer. According to several previous studies, placing a thin insulating layer between the base c-Si and ITO layers enhances the performance of the cell [14]. In this work, a thin insulating layer of Al_2O_3 was created between the boron-doped emitter and ITO via the atomic layer deposition (ALD) process, and its characteristics were examined. Thick poly-Si layers were substituted with thin nc-SiO_x(n) layers with thicknesses between 20 and 40 nm to minimize the parasitic absorption in these contacts. In this work, we used nc-SiO_x(n) instead of poly-Si to increase the transparency of the TOPCon solar cells. The nc-SiO_x(n) layer can not only enhance the electrical properties, but also increase the surface passivation, optical transmission, and carrier selectivity, all of which are important in device operation. nc-SiO_x(n) silicon films were fabricated via PECVD with phosphorus doping. Symmetrical lifetime samples were prepared to assess the junction characteristics and passivation quality of these nc-SiO_x(n)/SiO_x contacts based on their thicknesses. Furthermore, parasitic absorption losses in the nc-SiO_x(n) contacts were calibrated.

A representation of the proposed revolutionary solar cell technique is shown in Fig. 1. Our solar cell research aims were to: (a) establish a technique for improving cell performance using innovative structural methods; (b) use an innovative solar cell arrangement to attain an efficiency greater than 19%; (c) carry out substantial investigations on high-quality passivating contacts, such as nc-SiO_x(n)/SiO_x contacts; (d) provide a comprehensive experimental technique for manufacturing solar cells; (e) offer a technique for improving solar cell performance.

2. Materials and method

2.1. Preparation of symmetrical structure

The interface quality of the passivated rear contact on symmetrical nc-SiO_x(n)/SiO_x/c-Si(n)/SiO_x/nc-SiO_x(n) was measured by Quasi-steady-state photoconductance (QSSPC) system [15]. Symmetrical samples were prepared on commercially available n-type Cz wafers having a resistivity of 2–3 Ω-cm and thickness of 200 μm. Surface damage was removed using a heated potassium hydroxide (KOH) solution, and the sample was cleaned using Radio Corporation of America (RCA) chemicals. A thermal tube furnace was used to build a tunnel oxide (SiO_x) layer (~15 Å) on both sides of cleaned silicon wafer for 15 min at 700 °C with an O_2 flow rate of 10 L/min. Spectral ellipsometry revealed that the resultant tunnel oxide thickness was approximately 15 Å. Subsequently, phosphorus-doped nc-SiO_x (n) layers with thicknesses of approximately 20, 30, and 40 nm were synthesized on both surfaces using the PECVD tool of SNTEK company, with a frequency of 13.56 MHz. PECVD was used to deposit the material at a temperature of approximately 110 °C in the presence of silane (SiH_4), hydrogen (H_2), carbon dioxide (CO_2), and phosphine (PH_3) gases. A pressure of 1.5 T was used with a power of 35 mW/cm^2 for the deposition of the nc-SiO_x(n) layer. All fabricated samples were then subjected to post-deposition annealing (PDA) in an inert atmosphere at various temperatures of approximately 850, 900, 950, and 1000 °C/1 h for increased crystallization. The film thickness during the PECVD deposition of the nc-SiO_x(n) film, as well as the crystallization temperature, were varied to study their impact on the passivation quality. Finally, the QSSPC technique [16] was employed to determine the passivation quality by obtaining the implied V_{oc} (iV_{oc}) at the injection level of one sun based on the following equation:

$$iV_{oc} = \frac{kT}{q} \ln\left(\frac{\Delta n(\Delta n + N_D)}{n_i^2}\right), \quad (1)$$

where Δn represents an excess carrier density at one sun, T is the temperature, n_i being an intrinsic carrier density, k is the Boltzmann constant, N_D is the bulk doping density, and q is the elementary charge. The recombination current density (J_o) was extracted from the same measurements.

Conventional polysilicon passivated contact was produced as a reference. A symmetric sample was fabricated on planar commercial n-type CZ silicon wafers with a resistivity of 2–3 Ω-cm and thickness of 200 μm. Before the film deposition, the wafers were cleaned using a standard RCA procedure, followed by dipping in hydrofluoric acid (HF 10%) to remove the oxide from the wafer surfaces. Afterward, the wafers were loaded into a thermal tube furnace and annealed at the optimal temperature of 700 °C for 15 min in a gas mixture of nitrogen (N_2) and oxygen (O_2) to form a thin interfacial SiO_x layer with a thickness of ~15 Å. A reference sample was produced by depositing a 30 nm-thick, phosphorus-doped, hydrogenated amorphous silicon (n-a-Si: H) film on both sides of c-Si/SiO_x using PECVD. For the PECVD, SiH_4, H_2, and PH_3 were used as precursor gas sources for n-a-Si: H growth. After annealing at 950 °C in a N_2 environment for the dwell time of 60 min, reference sample was transformed into phosphorus-doped poly-Si layers (n + -poly-Si) on the c-Si/SiO_x structure (poly-Si/c-Si contact).

2.2. Device fabrication

N-type Si solar cells with a particular area of 10.24 cm^2 were fabricated on (2-3 Ω-cm, 200 μm thick) Cz wafers to examine the performance of the back-side tunnel oxide passivated contact in the final device (Fig. 1). Saw damage removal (SDR) was performed in a warm KOH solution by the alkaline texturing of silicon wafers throughout the manufacturing process. Subsequently, a mask was applied to the front to planarize the back. Suniva Inc. was used in the production line implanter to execute boron ion implantation with the appropriate dosage and energy. The lattice was then restored [17], and the boron-rich layer synthesis was eliminated [18] using higher-temperature annealing (>1000 °C). For emitter B, the resultant sheet resistivity was approximately 150 Ω/□. Using the same technique, the tunnel oxide and nc-SiO_x(n) layers were produced on the rear side. Al_2O_3 was deposited about 10 nm thick on the front side of the cell after a boron emitter using the ALD approach. In this study, an SiN_x film was replaced by sputtered ITO, which offers low sheet resistance and good conductivity for surface passivation and anti-reflection coating. Following this, ITO films with thicknesses of 100 and 130 nm were formed at the front and rear, respectively, using RF sputtering at a temperature of 180 °C. Finally, the solar cell was metalized with an Ag paste and a metal mesh that had screen printing on back and front sides, after which it was dried at 160 °C.

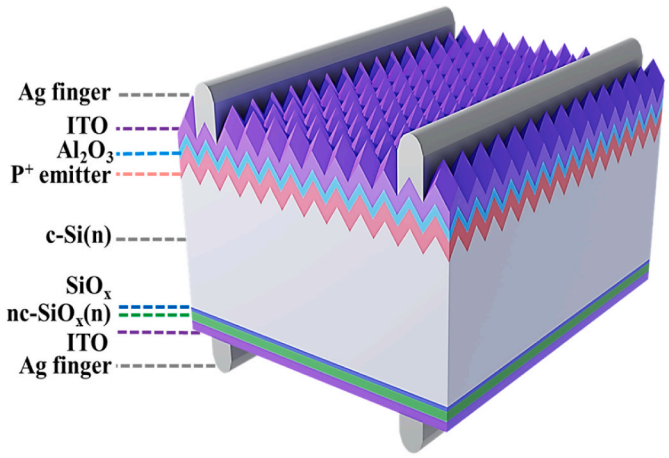

Fig. 1. Schematic diagram of proposed solar cell design.

2.3. Material characterization

Spectroscopic ellipsometry (VASE, JA Woollam) was used to validate the tunnel oxide and the nc-SiO_x(n) layer thicknesses. A QSSPC measuring system (WCT Sintron 120) was used to analyze the passivation properties. PECVD equipment from SNTEK and a thermal furnace from EM TECH were used within the experiment. To characterize the solar cells, their performance was evaluated under AM 1.5 illumination with a light intensity of 100 mW/cm^2 at 25 °C. All chemicals used within this experiment were synthesized by Duksan Pure Chemical, Korea.

3. Results and discussion

3.1. Passivation properties analysis

The passivation properties of nc-SiO_x(n) at the post-deposition annealing temperature (T_{PDA}) of 950 °C are shown in Fig. 2 as a function of thickness. PDA clarified the hydrogen transport in the c-Si substrate, disruption of the silicon-hydrogen bond, and phosphorous diffusion through the SiO_x layer in the n-type substrate. A tunnel oxide layer with ultrafine thickness was added to improve the passivation quality. The thermally annealed tunnel oxide junction cell structure exhibited good passivation properties. Passivation quality was degraded by heat treatment at 1000 °C. This is thought to be due to the local perturbation of the tunnel oxide layer. A bifacial structure was used to perform the QSSPC measurements. Followed by PDA, As the thickness of nc-SiO_x(n) layer approached 30 nm at 950 °C, notable enhancement in the passivation characteristics were observed. Fig. 2 depicts the iV_{oc}, minority carrier lifetime (τ_{eff}), and J_o of the deposited samples at an annealing temperature of 950 °C for various layer thicknesses. The improved chemical passivation of the ultrathin tunnel layer, owing to diminished field-effect passivation (FEP) due to carrier selectivity, can be linked to the particularly prominent enhancement in τ_{eff} and iV_{oc} as well as the reduction in J_o, with respect to the as-deposited nc-SiO_x(n) layer at an annealing temperature ~950 °C [19]. With maximal τ_{eff} and iV_{oc} of 2668 μs and 731 mV, respectively, and a nominal J_o of 3.1 fA/cm^2, the sample with a 30-nm-thick synthesized nc-SiO_x(n) layer after PDA at 950 °C demonstrated the best passivation characteristics.

The deposited 30-nm-thick nc-SiO_x(n) samples were annealed from 850 to 1000 °C temperature range. The passivation properties of the tunnel oxide junction structure were effective for samples that were thermally annealed at approximately 950 °C. The passivation quality, however, deteriorated with annealing above 950 °C, i.e., at 1000 °C. This phenomenon can be attributed to the local disturbance of SiO_x. Because of the minute area examination at the atomic scale, this damage was difficult to detect using transmission electron microscopy (TEM) and X-ray photoelectron spectroscopy (XPS) techniques. Bifacial structures were employed for QSSPC analysis. With the nc-SiO_x(n) layer thicknesses of 30 nm at 950 °C, substantial amelioration in passivation characteristics were observed following PDA. Fig. 3 shows the τ_{eff}, iV_{oc}, and J_o of the 30-nm-deposited samples based on the T_{PDA}. The outcomes of τ_{eff}, iV_{oc}, and J_o were improved when the annealing temperature was enhanced to 950 °C, and declined at further increase of annealing temperature. Particularly, increments in τ_{eff} and iV_{oc} and decrease in J_o in comparison with the as-deposited nc-SiO_x(n) layer at an annealing temperature of ~950 °C can be attributed to the improved chemical passivation of thin SiO_x owing to diminished FEP due to the carrier selectivity. The synthesized sample with the 30 nm nc-SiO_x(n) film after PDA of 950 °C had the most enhanced passivation properties, with a prominent lifetime and an iV_{oc} of approximately 2668 μs and 731 mV, respectively, and a minimum J_o of 3.1 fA/cm^2.

Fig. 4 displays plots of the τ_{eff}, iV_{oc}, and J_o values at the 30 nm nc-SiO_x(n) layer annealed at 950 °C, based on the [PH_3]/[SiH_4] gas ratio. As illustrated in Fig. 4, the exceptional passivation characteristics of the annealed sample appear in the medium doping level, with a high τ_{eff} of 2765 μs, an iV_{oc} of approximately 733 mV, and a low J_o of approximately 2.9 fA/cm^2. Beginning with low to medium doping levels, the τ_{eff} and iV_{oc} values steadily increased and then declined considerably at high doping levels. The opposite trend was observed in the J_o values. Moreover, the J_o trend suggests that the highly doped nc-SiO_x(n) layer might cause large recombination densities towards the nc-SiO_x(n)/c-Si interface, resulting in much higher J_o values. According to the results, optimal τ_{eff} and low J_o may be attained when dopants are restricted within the nc-SiO_x(n) film [20]. Therefore, significant diffusion of dopants within the c-Si bulk during the relaxation phase of thermal annealing is one of the causes of the low passivation quality at the heavily doped nc-SiO_x(n) layer.

Symmetrical cell structures were manufactured to investigate the quantitative influence of tunnel oxide layer on the passivation characteristics of proposed cell structure. Therefore, the intended structure had a tunnel oxide layer nc-SiO_x(n)/SiO_x/c-Si(n)/SiO_x/nc-SiO_x(n). The symmetrical test structure constituted an nc-SiO_x(n) layer of thickness 30 nm, with an optimal PH_3/SiH_4 ratio (medium doping level) of 1.5%, and an optimal annealing temperature of 950 °C. Fig. 5 depicts the injection-dependent effective τ_{eff} curves in favor of the symmetrical test structure with the tunnel oxide. The passivation parameters, including τ_{eff}, iV_{oc}, and J_o at 1×10^{15} (cm^{-3}), injection level, are shown for a particular structure. Fig. 5 clearly shows that a tunnel oxide layer with nc-SiO_x(n) is essential to achieve high-quality passivation. As the tunnel oxide layer provides a 4.5 eV obstacle for holes to cross a 3.1 eV threshold for electrons, the tunnel oxide layer is essential to the proposed structure allowing effective majority carrier (electron) transport,

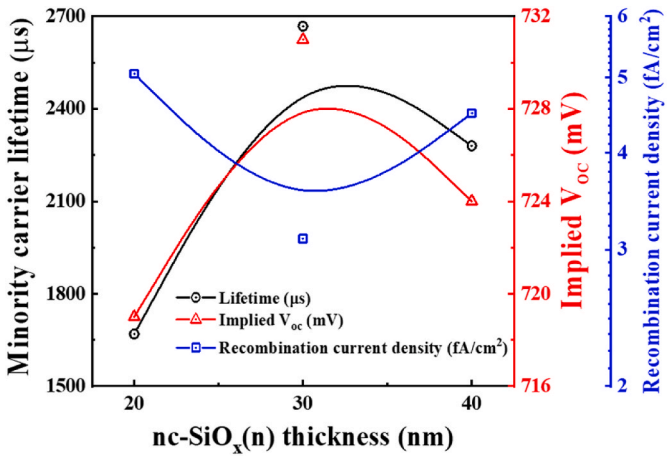

Fig. 2. Carrier lifetime, implied V_{oc}, and J_o fas a function of nc-SiO_x(n) thickness. QSSPC data were measured after annealing at 950 °C.

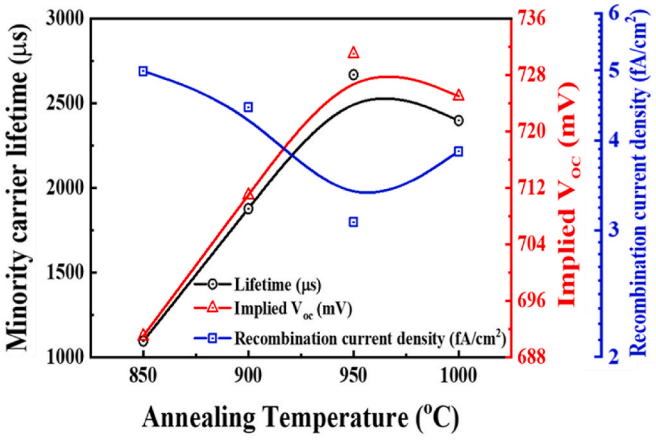

Fig. 3. Carrier lifetime, implied V_{oc}, and J_o at various temperatures.

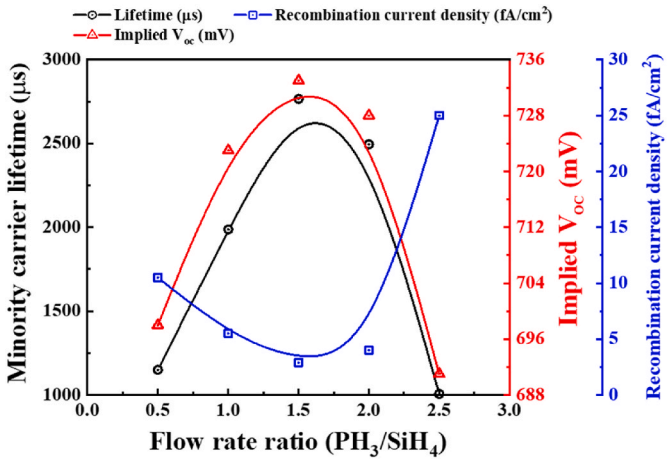

Fig. 4. Carrier lifetime, implied V_{oc}, and J_o as a function of doping variation.

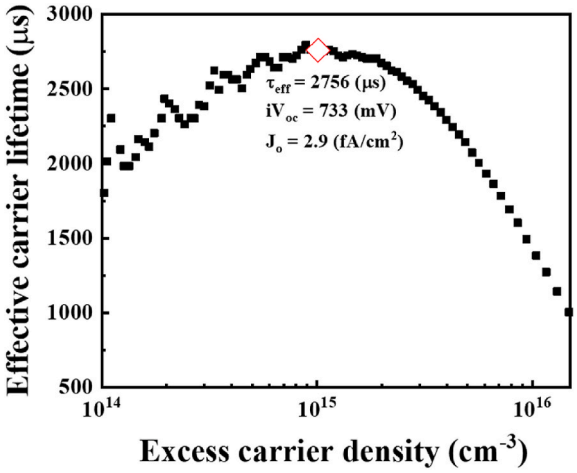

Fig. 5. Effective minority carrier lifetime for nc-SiO_x(n) (30 nm) symmetrically-passivated sample. The injection level at 1 × 10^{15} (cm^{-3}) and corresponding τ_{eff}, iV_{oc}, and J_o are also depicted.

while preventing minority carrier (hole) travel.

To investigate the influence of SiO_x/nc-SiO_x(n) passivated contacts, nc-SiO_x(n) layers were synthesized on the front and rear sides of the SiO_x layers, followed by forming gas annealing (FGA). J_o values were calculated using QSSPC analysis for the SiO_x/nc-SiO_x(n) passivating contacts, and the J_o values were calculated with QSSPC analysis. A significant improvement in the overall quality was realized following FGA on the passivated contact SiO_x/nc-SiO_x(n). The lowest values of J_o and $\rho_{contact}$ were obtained by thermal annealing at 950 °C along with FGA at 400 °C. The observations shown in Fig. 6 indicate that the overall $\rho_{contact}$ gradually decreased as the sample thickness increased, whereas the reduction was abrupt for the sample annealed at 950 °C. The lowest value of J_o obtained at 30-nm-thick nc-SiO_x(n) stack with SiO_x forming a passivated contact and annealed at 950 °C, demonstrated outstanding results compared to samples with alternative thicknesses. Passivated contact samples with diminished values (2.9 fA/cm^{-2}) at 30 nm, demonstrated restricted surface recombination along with improved passivation compared to that of the remaining thicknesses of 20 nm (21 fA/cm^{-2}) and 40 nm (9.5 fA/cm^{-2}). With a decrease in the J_o and $\rho_{contact}$ values, the tunneling efficiency was enhanced. Fig. 6 shows the J_o and $\rho_{contact}$ of the deposited samples with different nc-SiO_x(n) thicknesses in response to an annealing temperature of 950 °C.

Table 1 briefly reviews the comparison of the passivation properties of conventional polysilicon passivated contact (Poly-Si(n)/SiO_x/c-Si(n)) and nanocrystalline passivated contact (nc-SiO_x(n)/SiO_x/c-Si(n)). Comparison of the two passivating techniques, conventional polysilicon and nc-SiO_x(n) passivating contact might be an interesting approach. Indeed, due to its large thickness of poly-Si, the conventional TOPCon structure causes significant parasitic absorption, which is a significant issue when it comes to the front or back contact. To tackle this problem, we come up with a thin layer of nc-SiO_x(n) which provides better passivation as well as low parasitic absorption. A SiO_x, on the other hand, has a lot of potential because of its high passivation. As a result, a nc-SiO_x(n) with a tunnel passivated contact may be considered as prominent than reference one.

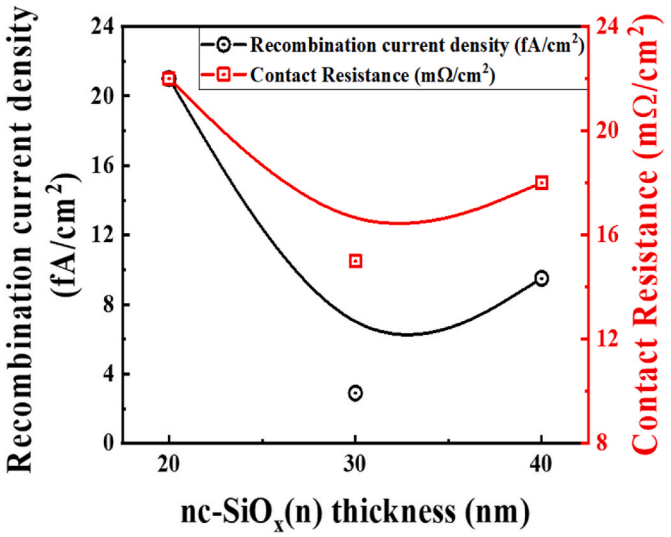

Fig. 6. Contact resistance ($\rho_{contact}$) with J_o for various nc-SiO_x(n) layer thicknesses.

Table 1
Passivation parameter of nc-SiO_x(n)/SiO_x/c-Si(n) and Poly-Si(n)/SiO_x/c-Si(n) symmetrically passivated sample and Contact resistance. The injection level at 1 × 10^{15} (cm^{-3}) and corresponding τ_{eff}, iV_{oc}, J_o and $\rho_{contact}$ are also depicted.

Structure	τ_{eff} (μs)	iV_{oc} (mV)	J_o (fA/cm^2)	$\rho_{contact}$ (mΩ/cm^2)
nc-SiO_x(n)/SiO_x/c-Si(n)	2756	733	2.9	15
Poly-Si(n)/SiO_x/c-Si(n) (Reference)	2150	717	10.75	20

3.2. Assessment of solar cell results

Fig. 7(a–d) depict the characteristics acquired from the J-V measurements of the solar cells, including nc-SiO_x(n) layer different thicknesses. Fig. 7(a) shows the open-circuit voltage (V_{oc}) values based on nc-SiO_x(n) thickness, which exhibit an increase up to a maximum of 657 mV supporting a 40 nm nc-SiO_x(n). Furthermore, the short-circuit current (J_{sc}) demonstrates a similar trend based on the nc-SiO_x(n) layer thickness (Fig. 7(b)), that is, a maximum for 20 nm nc-SiO_x(n) and a reduction with increasing thickness. This may be attributed to the optimal condition across a particular 30 nm nc-SiO_x(n), where $\rho_{contact}$ due to the passivation layer is minimized. Furthermore, the nc-SiO_x(n) layer thickness influences not only carrier transport but also resistivity loss; therefore, the FF value is optimal. Furthermore, the nc-SiO_x(n) layer influences the FF by modulating carrier transit and resistance. As illustrated in Fig. 7(c), an optimal FF of 78% was achieved supporting the intermediate 30 nm nc-SiO_x(n). The FF was degraded by thinner or thicker nc-SiO_x(n) layers instead of the layer with 30 nm thickness. Moreover, a discrepancy was observed between iV_{oc} and cell V_{oc}, that is, iV_{oc} > V_{oc} in all cases. However, modeling demonstrated that an

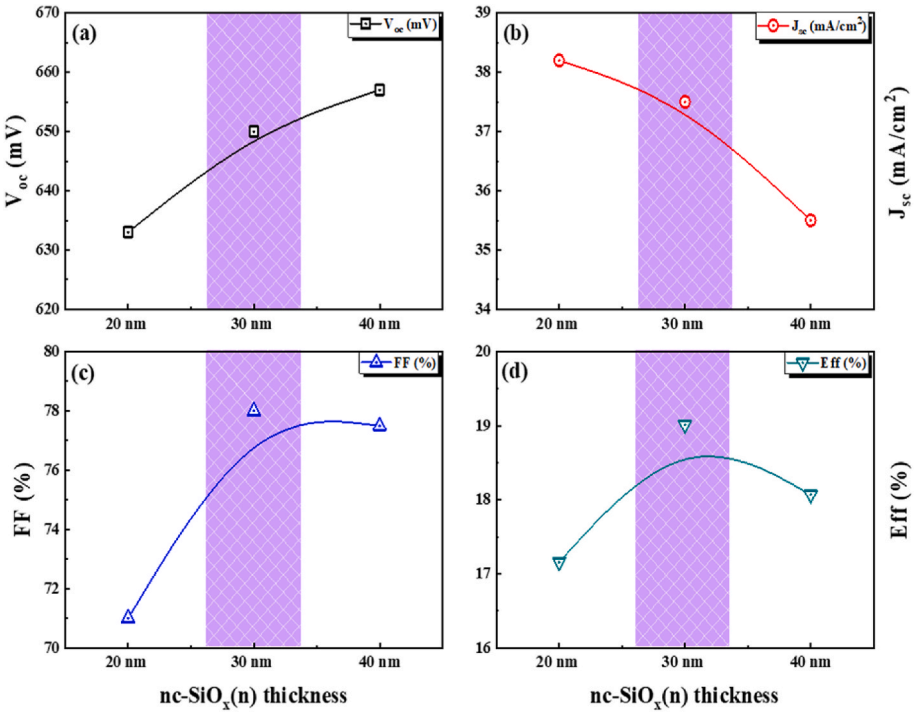

Fig. 7. Solar cell measurements: (a) V_{oc}, (b) J_{sc}, (c) FF, and (d) E_{ff} based on the film thickness for the rear side nc-SiO$_x$(n) layers. The highlighted sections represent the best outcomes.

irradiation intensity-dependent iV_{oc} assessment is a realistic upper limit for the attainable V_{oc} for industrial devices. Furthermore, the V_{oc} measurement represents the excess carrier density of the cell with metallization, which may cause shading and iV_{oc} in non-metalized regions. Another reason for the large discrepancy might be metal damage, either due to blistering or spiking. The final optimized efficiency of a cell was found to be 19.01% for a thin 30 nm nc-SiO$_x$(n), as shown in Fig. 7(d). Table 1 summarizes the measured J-V characteristics of the nc-SiO$_x$(n)-based solar cells in favor of the leading cells per variation, along with the averaged data. Cell manufacturing was repeated four times to ensure that both the experimental techniques and the cells were stable. We evaluated our optimized cell five times under the same conditions to investigate the measurement uncertainty, and the percentage of error was reported, as shown in Table 1.

The most important parameter to describe a silicon solar cell is its current density dependence on the applied voltage, which is generally represented as the J-V curve. Fig. 8 depicts the J-V features of the solar cells with different nc-SiO$_x$(n) layer thicknesses. nc-SiO$_x$(n) films with thicknesses of approximately 20, 30, and 40 nm were used to fabricate the solar cells. The thickness of nc-SiO$_x$(n) layer had an appropriate effect on the cell results, as shown in Fig. 7. When the 30 nm nc-SiO$_x$(n) film thickness was applied, the highest result attained by the silicon solar cell were V_{oc} = 650 mV, J_{sc} = 37.5 mA/cm^2, FF = 78%, and = 19.01%. Additionally, with the enhancement of nc-SiO$_x$(n) thickness from 20 nm to 30 nm, J_{sc} was reduced to 37.5%, followed by a huge enhancement in V_{oc}; nevertheless, FF improved moderately from 71% to 78%. V_{oc} was enhanced by the layer thickness of nc-SiO$_x$(n) since the higher Fermi level and wider optical bandgap (E_g) resulted in an increase in built-in voltage. Furthermore, the wide E_g of the nc-SiO$_x$(n) layer improved J_{sc} by reducing the series resistance and permitting light further into the c-Si substrate. Additionally, the light absorption losses induced by increasing the nc-SiO$_x$(n) layer thickness largely offset this gain, which may explain why J_{sc} degrades slightly with an increase in the layer thickness.

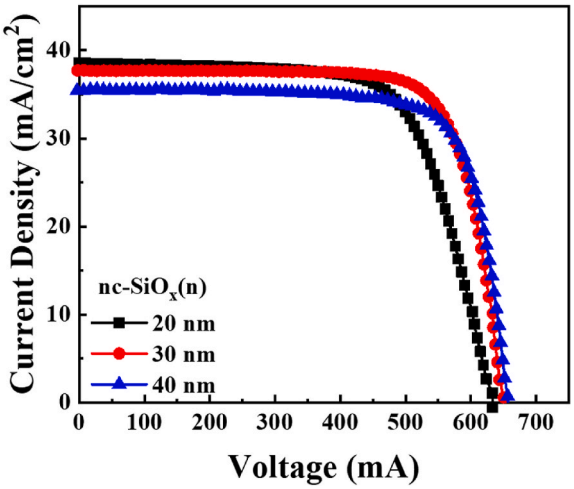

Fig. 8. J-V characteristics of cells with various nc-SiO$_x$(n) thicknesses.

The highest power conversion efficiency (PCE) of 19.01% was achieved for the solar cell with 30 nm of nc-SiO$_x$(n) layer. J_{sc}, FF, and η degraded dramatically for the 30–40 nm nc-SiO$_x$(n) layer, and a corresponding reduction in the performance of the silicon solar cell was recorded. Due to poor quality of the nc-SiO$_x$(n) layer at 10 nm thickness, solar cells accompanied by a 10 nm layer exhibited low efficiency. The probability of recombination increased with the thickness of the nc-SiO$_x$(n) layer because the charge carriers must travel farther to reach the collecting electrodes. Finally, the best performance of V_{oc} = 650 mV, J_{sc} = 37.5 mA/cm^2, FF = 78%, and FF = 19.01% was recorded for nc-SiO$_x$(n) layer with 30 nm thickness. Table 2 summarizes the calculated J-V parameters of the silicon solar cells for the optimized cells, along with the averaged data. Cell manufacturing was repeated four times to ensure that the experimental techniques and cells were both stable. We evaluated our optimized cell five times under identical conditions to investigate the measurement uncertainty, and a small percentage of error was detected, as shown in Table 1. Further research is being conducted to overcome these difficulties, whereby the results will be

Table 2
Repetition and summarizes the calculated J-V parameters of the silicon solar cells for the optimized cells under 1-sun irradiation (100 mW/cm^2).

Structure	V_{oc} (mV)	J_{sc} (mA/cm^2)	FF (%)	η (%)
Best silicon solar cell	650 ± 0.002	37.5 ± 0.4	78 ± 0.002	19.01 ± 0.3
Avg. for 5 silicon solar cells	649.5 ± 0.5	37.2 ± 0.3	77.4 ± 0.6	18.61 ± 0.4

revealed in due course.

4. Conclusion

High-performance n-type Si solar cells with an innovative cell design were presented. nc-SiO_x(n)/SiO_x passivated contacts formed by PECVD deposition, and a thermal furnace were demonstrated. Future developments might benefit from ITO being deposited on top of solar cells because it preempts complex procedures and uses less material. In this work, a very thin layer of Al_2O_3 created by ALD was added before the ITO layer deposition. The Al_2O_3 layer served well and increased the carrier density of the cell. It was demonstrated that the passivation quality of our passivated contact scheme heavily influenced on annealing temperature and thickness. Optimization of the process parameters enabled an iV_{oc} as high as 733 mV with a corresponding J_o value of 2.9 fA/cm^2, suggesting an excellent interface passivation quality of 30 nm nc-SiO_x(n). Furthermore, the simple solar cells with a boron emitter, passivation layer, and ITO on front/rear nc-SiO_x(n)/SiO_x contacts demonstrated that these are efficient carrier-selective contacts, thereby permitting V_{oc} of 650 mV, including FF>78%. In conclusion, the solar cell results demonstrate that parasitic absorption is less prominent in nc-SiO_x(n) films than in poly-Si films. The completed cells with tunnel oxide passivated rear contact demonstrated average cell efficiency greater than 19% after screen-printed metallization on an ITO, highlighting the potential of this technique to produce future high-performance solar cells.

CRediT authorship contribution statement

Muhammad Quddamah Khokhar: Writing – original draft, Investigation, Formal analysis, Data curation, Conceptualization. **Shahzada Qamar Hussain:** Writing – review & editing, Investigation, Formal analysis, Data curation. **Youngkuk Kim:** Writing – review & editing, Investigation, Formal analysis, Data curation. **Suresh Kumar Dhungel:** Data curation, Formal analysis, Investigation, Writing – review & editing. **Junsin Yi:** Visualization, Supervision, Project administration, Investigation, Funding acquisition.

Declaration of competing interest

The authors declare that they have no known competing financial interests or personal relationships that could have appeared to influence the work reported in this paper.

Data availability

Data will be made available on request.

Acknowledgment

This research was supported by grants from the Korea Institute of Energy Technology Evaluation and Planning (KETEP) funded by the Korean Ministry of Trade, Industry, and Energy (MOTIE) [grant numbers 20218520010100, 20203040010320].

References

[1] M. Taguchi, A. Yano, S. Tohoda, K. Matsuyama, Y. Nakamura, T. Nishiwaki, K. Fujita, E. Maruyama, 24.7% record efficiency HIT solar cell on thin silicon wafer, IEEE J. Photovoltaics 4 (2013) 96–99.
[2] E. Yablonovitch, T. Gmitter, R.M. Swanson, Y.H. Kwark, A 720 mV open circuit voltage SiO x: c-Si: SiO x double heterostructure solar cell, Appl. Phys. Lett. 47 (1985) 1211–1213.
[3] F. Feldmann, M. Bivour, C. Reichel, M. Hermle, S.W. Glunz, Passivated rear contacts for high-efficiency n-type Si solar cells providing high interface passivation quality and excellent transport characteristics, Sol. Energy Mater. Sol. Cells 120 (2014) 270–274.
[4] M.Q. Khokhar, S.Q. Hussain, S. Chowdhury, M.A. Zahid, D.P. Pham, S. Jeong, S. Kim, S. Kim, E.-C. Cho, J. Yi, High-efficiency hybrid solar cell with a nanocrystalline silicon oxide layer as an electron-selective contact, Energy Convers. Manag. 252 (2022), 115033.
[5] S.W. Glunz, F. Feldmann, A. Richter, M. Bivour, C. Reichel, H. Steinkemper, J. Benick, M. Hermle, The irresistible charm of a simple current flow pattern–25% with a solar cell featuring a full-area back contact, in: Proc. 31st Eur. Photovolt. Sol. Energy Conf. Exhib., München WIP, 2015, pp. 259–263.
[6] D. Adachi, J.L. Hernández, K. Yamamoto, Impact of carrier recombination on fill factor for large area heterojunction crystalline silicon solar cell with 25.1% efficiency, Appl. Phys. Lett. 107 (2015), 233506.
[7] K. Masuko, M. Shigematsu, T. Hashiguchi, D. Fujishima, M. Kai, N. Yoshimura, T. Yamaguchi, Y. Ichihashi, T. Mishima, N. Matsubara, Achievement of more than 25% conversion efficiency with crystalline silicon heterojunction solar cell, IEEE J. Photovoltaics 4 (2014) 1433–1435.
[8] U. Römer, R. Peibst, T. Ohrdes, B. Lim, J. Krügener, T. Wietler, R. Brendel, Ion implantation for poly-Si passivated back-junction back-contacted solar cells, IEEE J. Photovoltaics 5 (2015) 507–514.
[9] F. Feldmann, R. Müller, C. Reichel, M. Hermle, Ion implantation into amorphous Si layers to form carrier-selective contacts for Si solar cells, Phys. Status Solidi Rapid Res. Lett. 8 (2014) 767–770.
[10] C. Reichel, F. Feldmann, R. Müller, R.C. Reedy, B.G. Lee, D.L. Young, P. Stradins, M. Hermle, S.W. Glunz, Tunnel oxide passivated contacts formed by ion implantation for applications in silicon solar cells, J. Appl. Phys. 118 (2015), 205701.
[11] G. Yang, A. Ingenito, N. van Hameren, O. Isabella, M. Zeman, Design and application of ion-implanted polySi passivating contacts for interdigitated back contact c-Si solar cells, Appl. Phys. Lett. 108 (2016), 33903.
[12] M. Rienäcker, A. Merkle, U. Römer, H. Kohlenberg, J. Krügener, R. Brendel, R. Peibst, Recombination behavior of photolithography-free back junction back contact solar cells with carrier-selective polysilicon on oxide junctions for both polarities, Energy Proc. 92 (2016) 412–418.
[13] F. Ruske, Deposition and properties of TCOs, in: Phys. Technol. Amorph. Heterostruct. Silicon Sol. Cells, Springer, 2012, pp. 301–330.
[14] S.J. Fonash, Outline and comparison of the possible effects present in a metal–thin–film–insulator–semiconductor, J. Appl. Phys. 47 (1976) 3597–3602.
[15] R.A. Sinton, A. Cuevas, M. Stuckings, Quasi-steady-state photoconductance, a new method for solar cell material and device characterization, in: Conf. Rec. Twenty Fifth IEEE Photovolt. Spec. Conf., IEEE, 1996, pp. 457–460.
[16] D.E. Kane, R.M. Swanson, Measurement of the emitter saturation current by a contactless photoconductivity decay method, IEEE Photovolt. Spec. Conf. 18 (1985) 578–583.
[17] M. Hermle, J. Benick, M. Rüdiger, N. Bateman, S.W. Glunz, N-type silicon solar cells with implanted emitter, in: 26th Eur. Photovolt. Sol. Energy Conf. Hamburg, Ger., 2011, pp. 875–878.
[18] Y. Tao, A. Rohatgi, High-efficiency large area ion-implanted n-type front junction Si solar cells with screen-printed contacts and SiO_2 passivated boron emitters, in: IEEE 40th Photovolt. Spec. Conf., IEEE, 2014, pp. 3654–3658, 2014.
[19] M.-A.N. Eyoum, Modularly Integrated MEMS Technology, CALIFORNIA UNIV BERKELEY DEPT OF ELECTRICAL ENGINEERING AND COMPUTER SCIENCE, 2006.
[20] G. Yang, A. Ingenito, N. van Hameren, O. Isabella, M. Zeman, Design and application of ion-implanted polySi passivating contacts for interdigitated back contact c-Si solar cells, Appl. Phys. Lett. 108 (2016), 33903.